

General theory of Josephson Diodes

Yi Zhang,^{1,2} Yuhao Gu,³ Jiangping Hu,^{3,2,*} and Kun Jiang^{3,†}

¹*Department of Physics, Shanghai University, Shanghai 200444, China*

²*Kavli Institute of Theoretical Sciences, University of Chinese Academy of Sciences, Beijing, 100190, China*

³*Beijing National Laboratory for Condensed Matter Physics and Institute of Physics, Chinese Academy of Sciences, Beijing 100190, China*

(Dated: January 10, 2022)

Motivated by recent progress in the superconductivity nonreciprocal phenomena, we study the general theory of Josephson diodes. The central ingredient for Josephson diodes is the asymmetric proximity process inside the tunneling barrier. From the symmetry breaking point of view, there are two types of Josephson diodes, inversion breaking and time-reversal breaking. For the inversion breaking case, applying voltage bias could effectively tune the proximity process like the voltage-dependent Rashba coupling giving rises to $I_c(V) \neq I_c(-V)$. For the time-reversal breaking case, the magnetic field and current flow could adjust the internal time-reversal breaking field like magnetism or time-reversal breaking electron-electron pairing, which leads to $I_c(B) \neq I_c(-B)$ or $I_{c+} \neq I_{c-}$. All these results provide a complete understanding and the general principles of realizing Josephson diodes, especially the recently found $\text{NbSe}_2/\text{Nb}_3\text{Br}_8/\text{NbSe}_2$ Josephson diodes.

As a macroscopic quantum phenomenon, superconductivity is one of the most important subjects in condensed matter physics [1–3]. The central ingredients for a superconductor (SC) are the electron-electron pairing and phase coherence, which gives rise to the absence of resistivity and the Meissner effect. Brian Josephson elegantly linked the pairing condensation and phase coherence with the supercurrent generation between two weak-linked superconductors, which is now known as the Josephson effect or Josephson junction [4, 5]. The emergence of the Josephson effect enables the wide applications of superconductivity, like the superconducting quantum interference device etc.

However, compared with modern semiconductor electronic devices, the devices based on superconducting current are still very limited. For the normal electric current, a semiconductor p-n junction, known as the diode, conducts current primarily in one direction. This non-reciprocal charge transport has multiple usages including rectification of current, detection of radio signals etc., which makes the diode becoming one of the key devices in the semiconductor industry [6]. Thus, in order to broaden the potential application of the superconducting current, we can ask a natural question: is there a diode for the superconducting current? We will name such a diode as Josephson diode.

Historically, the first theoretical proposal for Josephson diodes stems from the SC analogy of p-n junctions by the electron and hole doped SCs close to an SC-Mott-insulator transition [7]. Recently, the nonreciprocal Josephson effect utilizing the charging asymmetry effect has been studied by semiclassical approaches [8]. Using the magnetochemical anisotropy, the non-reciprocal responses and superconducting diode effects under the external magnetic field have been investigated both theoretically and experimentally [9–14]. Similarly, the asymmetric Fermi velocities of topological materials edge states under external magnetic fields have also been proposed to have a nonreciprocal effect [15].

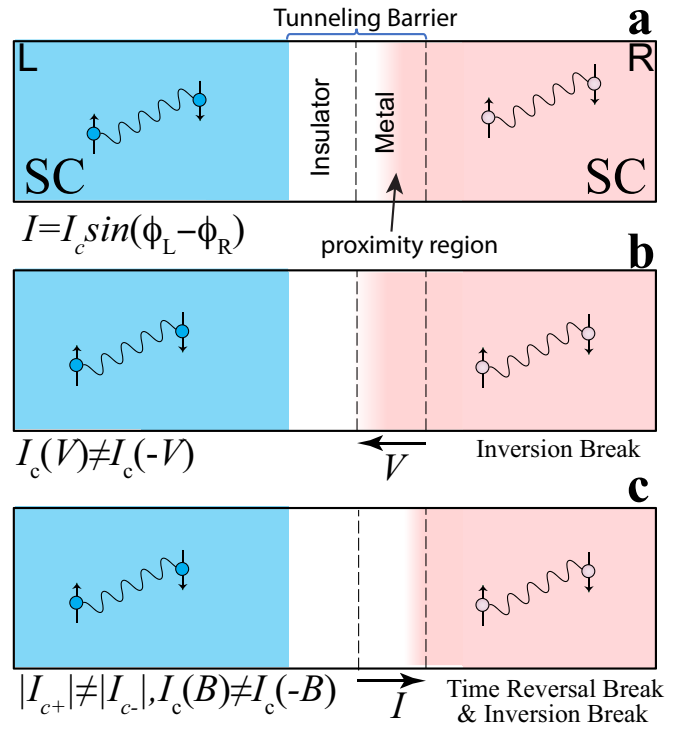


FIG. 1. **a**, The geometric setup for a Josephson diode in an extreme limit, which is formed by SC Δ_L on the left, SC Δ_R on the right and the tunneling barrier (TB). The Josephson current is determined by $I = I_c \sin(\phi_L - \phi_R)$, where $\phi_{L/R}$ is the phase and I_c is the critical current. The tunneling barrier layer in the extreme limit is formed by an insulator layer and a metallic layer (N). And the Δ_R influences the N layer by forming the proximity region. **b**, An inversion breaking JD is controlled by voltage with $I_c(V) \neq I_c(-V)$, which effectively adjusts the proximity region. **c**, A time reversal breaking JD (with inversion breaking) controlled by current flow I with $I_{c+} \neq I_{c-}$, where \pm represents the flow direction. Similarly, the diodes can also be controlled by the magnetic field with $I_c(B) \neq I_c(-B)$.

Most recently, a Josephson diode without a magnetic field has been observed in an inversion asymmetric $\text{NbSe}_2/\text{Nb}_3\text{Br}_8/\text{NbSe}_2$ (NSB) heterostructure [16], where the critical current in the positive direction deviates from the neg-

ative one. The experiment goes beyond the above theoretical considerations. Thus it calls for a broader theory for the Josephson diode.

In this work, we show that there are two types of Josephson diodes (JDs), inversion breaking JD and time reversal breaking JD, as illustrated in Fig.1. The inversion breaking JD can be controlled by voltage bias, similar to the first proposal in Ref.[7]. The time-reversal breaking JD can be controlled by a magnetic field or the current flow etc. As shown in Fig.1a, a Josephson diode is formed by a tunneling barrier (TB) and two SCs on the left (Δ_L) and the right (Δ_R) respectively. The minimal symmetry requirement for forming a diode is the inversion symmetry breaking. Therefore, the coupling between TB and Δ_L must be different from the coupling between TB and Δ_R . To simplify our discussion, we will take an extreme limit, where the TB layer is formed by an insulator layer and a metallic layer (N), as illustrated in Fig.1a. And the Nb_3Br_8 barrier in Ref. [16] NSB heterostructure indeed belongs to this case, which will be discussed below [17]. Owing to the metallic nature, the Δ_R will induce superconducting pairing into the N layer by generating an SC proximity region as illustrated in Fig.1a. This SC proximity region can be served as the effective “depletion” region as in the semiconductor p-n junction. Clearly, tuning the proximity region is equivalent to tuning the effective length of TB and the Josephson coupling between Δ_L and Δ_R . Hence, if we can control this proximity region, a Josephson diode can be easily realized as illustrated in Fig.1b,c.

From the symmetry point of view, the above structure breaks the inversion symmetry \mathcal{I} when other symmetries of the TB layer are not specified. Owing to Onsager reciprocal relations, the nonreciprocal response can occur under an \mathcal{I} breaking field, for example the external voltage bias (V). On the other hand, the magnetic field (B) and current flow (I) break the time reversal symmetry \mathcal{T} . Taking current flow as an example, the Hamiltonian of any \mathcal{T} invariant system at positive current $\hat{H}(+I)$ is related to the negative one $\hat{H}(-I)$ by a \mathcal{T} operation, which ensures $I_{c+} = -I_{c-}$. Therefore, to have the nonreciprocal response for B and I, the TB layer must additionally break the \mathcal{T} symmetry. In the following, we will discuss each of them respectively.

Inversion breaking For an \mathcal{I} breaking JD, the essential part is a voltage-dependent quantity. In the conventional p-n junctions, the depletion region is formed by diffusion between electrons from n-doped region and holes from the p-doped region. Then, the built-in potential between holes and electrons inside the depletion region competes with the external voltage giving rise to the nonreciprocal transport. The Josephson diode using the hole and electron-doped SC is also based on the similar built-in potential by electrons and holes, where the depletion region is formed by a self-organized Mott insulator region [7]. This JD belongs to the \mathcal{I} breaking Josephson diode [7]. Additionally, there are many other quantities that can be controlled by voltage, for example the Rashba spin orbital coupling (SOC) $\alpha\boldsymbol{\sigma} \times \mathbf{p}$ [18–21]. Since the Rashba coupling α is proportional to the interfacial electric field $E \propto -\nabla V$,

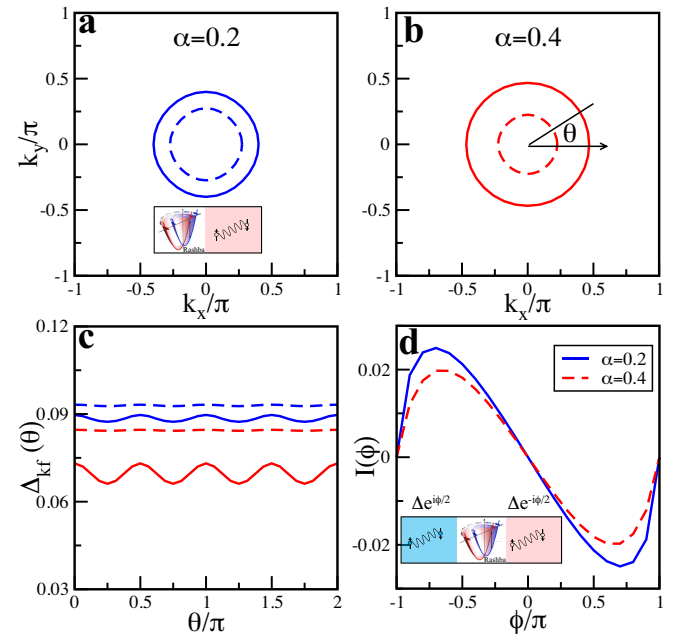


FIG. 2. **a**, Fermi surface for TB with $\alpha = 0.2$. The inset illustrates the proximity process leading to the pairing amplitude in **c**. **b**, Fermi surface for TB with $\alpha = 0.4$. **c**, Spin singlet pairing strengths along each FS for $\alpha = 0.2, 0.4$. θ is the angle along each FS as defined in **a**, **b**. **d**, The Josephson currents $I(\phi)$ in unit of $\frac{2e}{h}$ for the Rashba JD for $\alpha = 0.2$ and $\alpha = 0.4$ and the inset shows the setup for calculating the current. The other parameters are set as $t_R = t_L = 1.0$, $\Delta_R = \Delta_L = 0.2$, $t_{RB} = 0.8$, $t_{LB} = 0.6$, $\mu = -3.0$. In the calculation, we set the thickness of SC on both sides to be 20.

applying a voltage, in turn, could change the magnitude of α [20, 22, 23]. And the magnitude of α will influence the proximity region owing to the changing of Fermi momentum k_F and the spin texture along the Fermi surfaces (FSs).

To justify this theory, we start from the proximity process between the right SC Δ_R and TB with Rashba SOC, as illustrated in Fig.2a. The Hamiltonian can be written as $H_0 = H_R + H_{TB} + H_{RTB}$. The H_R describes the right SC with a cubic lattice and the s-wave pairing for the spinor $c_i = (c_{i,\uparrow}, c_{i,\downarrow})^T$ as

$$H_R = -t_R \sum_{\langle ij \rangle} c_i^\dagger c_j + \Delta_R \sum_i c_{i\uparrow} c_{i\downarrow} + h.c. \quad (1)$$

The H_{TB} describes the TB layer with a square lattice and rashba SOC for the spinor $f_i = (f_{i,\uparrow}, f_{i,\downarrow})^T$ as

$$H_{TB} = -t_{TB} \sum_{\langle ij \rangle} f_i^\dagger f_j - i\alpha \sum_{\langle ij \rangle} f_i^\dagger (\boldsymbol{\sigma} \times \mathbf{d}_{ij})_z f_j + h.c. \quad (2)$$

where the \mathbf{d}_{ij} is the unit vector from site i to site j. The coupling between them is described by H_{RTB} as

$$H_{RTB} = -t_{RB} \sum_{\langle ij \rangle} f_i^\dagger c_j + h.c. \quad (3)$$

Owing to Rashba SOC, the spin-degenerate FSs split into two helical FSs with spin-momentum locking as $\boldsymbol{\sigma} \times \mathbf{k}$. The δk_F

difference between two split FSs depends on the magnitude of α . By comparing the FSs at Fig.2a,b, we can find δk_F for $\alpha = 0.2$ is smaller than $\alpha = 0.4$. Then, we can compare the effective pairing strength $\langle f_{k\uparrow}^\dagger f_{-k\downarrow}^\dagger \rangle$ for each proximity process. The effective pairing $\Delta(\theta)$ s along the TB FSs in Fig.2c show that $\alpha = 0.2$ obtains a much larger pairing than $\alpha = 0.4$. Normally, the proximity process between metal and SC is coming from the Andreev reflection [24, 25]. The mismatching between the metal k_F and SC momentum gives rise to this pairing strength difference between different α . Since the k_F of $\alpha = 0.2$ is much closer to the k_F of Δ_R , a much larger pairing is obtained. Hence, adjusting Rashba SOC can efficiently adjust the proximity region.

To calculate the Josephson effect, we still need to couple H_0 with the left part Δ_L . The Hamiltonian H_L is similar to H_R as

$$H_L = -t_L \sum_{\langle ij \rangle} c_i^\dagger c_j + \Delta_L \sum_i c_{i\uparrow} c_{i\downarrow} + h.c. \quad (4)$$

And the coupling with TB is written as

$$H_{LTB} = -t_{LB} \sum_{\langle ij \rangle} f_i^\dagger c_j + h.c. \quad (5)$$

The inversion symmetry breaking can be simulated by $t_{LB} \neq t_{RB}$. It seems that this setup ignores the insulator layer. However, setting $t_{LB} \neq t_{RB}$ is just equivalent to integrating out the insulator layer degree of freedom. We can further introduce a phase into the SCs as $\Delta_L = \Delta_0 e^{i\phi/2}$ and $\Delta_R = \Delta_0 e^{-i\phi/2}$. Then the supercurrent through the junction is related to the total Hamiltonian $H_t = H_0 + H_L + H_{LB}$ by

$$I(\phi) = -\frac{2e}{\hbar} \partial_\phi \sum_n f(\epsilon_n) \epsilon_n(\phi) \quad (6)$$

where the ϵ_n is the n-th eigenvalue for H_t at the phase ϕ [10, 26]. The $I(\phi)$ is calculated as the function of ϕ in Fig.2d. The results in Fig.2d demonstrate the critical current I_c for Rashba Josephson junction decreases with increasing the α SOC. Therefore, a voltage controlled JD with $I_c(V) \neq I_c(-V)$ can be realized by the voltage dependent Rashba SOC. The external voltage competes with the internal interfacial voltage at the interfaces, leading to a tunable Rashba SOC.

Time reversal breaking As discussed above, there is another type of JD by further breaking \mathcal{T} symmetry. To achieve this goal, the TB layer must break \mathcal{T} owing to Onsager reciprocal relations. The simplest \mathcal{T} breaking phenomenon in solid state physics is magnetism. Hence, assuming the TB layer contains the internal magnetism, if the proximity region can be tuned by tuning the magnetization amplitude, a \mathcal{T} breaking JD can be achieved.

To simulate this magnetic order, we can add a double-exchange coupling term $M \sum_i f_i^\dagger \sigma_z f_i$ [27, 28] into the microscopic Hamiltonian H_{TB} . Just as above, we first investigate the proximity process. Since magnetism disfavors spin-singlet pairing, a larger M should weaken the proximity effect. By comparing the FSs at different M at Fig.3a,b, the spin split

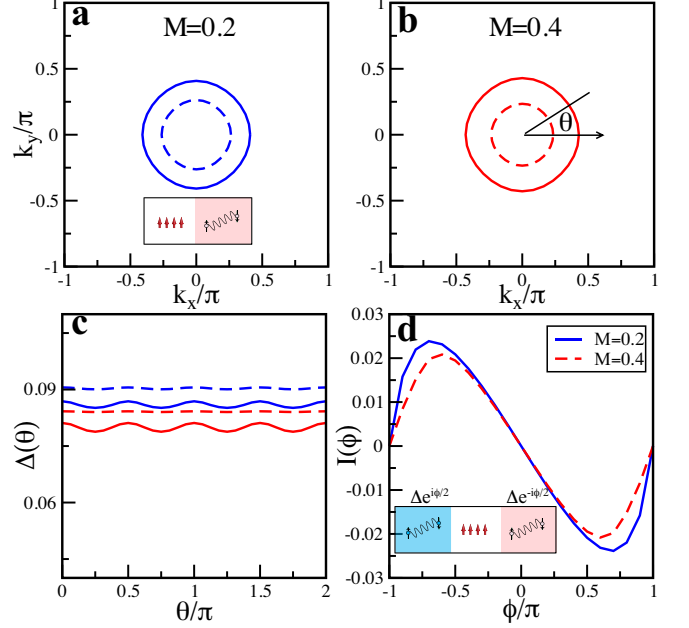


FIG. 3. **a**, Fermi surface for TB with $M = 0.2$. The inset illustrates the proximity process leading to the pairing amplitude in **c**. **b**, Fermi surface for TB with $M = 0.4$. **c**, Spin singlet pairing strengths along each FS for $M = 0.2, 0.4$. θ is the angle along each FS as defined in **a**, **b**. **d**, The Josephson currents $I(\phi)$ in unit of $\frac{2e}{\hbar}$ for the magnetic JD for $M = 0.2$ and $M = 0.4$ and the inset shows the setup for calculating the current. The other parameters are set as $t_R = t_L = 1.0$, $\Delta_R = \Delta_L = 0.2$, $t_{RB} = 0.8$, $t_{LB} = 0.6$, $\alpha = 0.2$, $\mu = -3.0$. In the calculation, we set the thickness of SC on both sides to be 20.

FSs at $M = 0.2$ are slightly different than that at $M = 0.4$ with an even larger δk_F . From Fig.3c, the effective singlet pairing strength along the TB FS for $M = 0.2$ is larger than the case with $M = 0.4$. Hence, if the external magnetic field could change the value of M , the proximity region can be adjusted. The Josephson current of the above JD can be also calculated by Eq.(6). From Fig.3d, the critical current I_c for $M = 0.2$ is larger than the case with $M = 0.4$. Therefore, a $I_c(B) \neq I_c(-B)$ time reversal breaking JD can be achieved by the external magnetic field and the magnetic order inside the TB layer.

Besides the magnetic field-controlled JD, the current flow is another efficient way towards realizing the \mathcal{T} breaking JD. Especially, the most striking phenomenon in NSB heterostructure is the nonreciprocal transport depending on the current direction [16]. Since current breaks \mathcal{T} symmetry, the TB layer must break \mathcal{T} symmetry for a current controlled JD. For example, the TB layer can host \mathcal{T} breaking superconducting at low temperatures. Normally, \mathcal{T} breaking SC can happen as an instability driven by multiple order competition and correlation, like the $d + id$ SC in 1/4 doped graphene [29, 30] and the $d + is$ SC when a d-wave SC coexists with an s-wave SC [31–33]. For simplicity, we take a $d + is$ wave SC in the TB layer as an example by assuming TB favors a d-wave SC owing to correlation. More general cases for pure is , $s + ip$ etc.

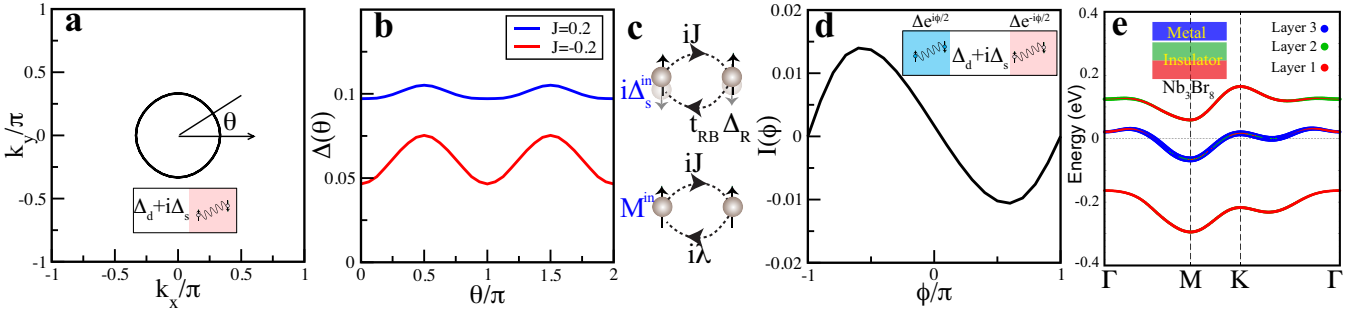


FIG. 4. **a**, Fermi surface for TB with $\Delta_d + i\Delta_s$ pairing. The inset illustrates the proximity process leading to the pairing amplitude in **b**. **b**, Spin singlet pairing strengths along each FS for $J = \pm 0.2$. θ is the angle along each FS as defined in **a**. **c**, Perturbation process for pairing and magnetism respectively. In the top panel, a current term $iJf_i c_j^\dagger$, a pairing term $c_{j\sigma}^\dagger c_{j\sigma}^\dagger$ followed by $t_{RBC} f_i^\dagger$ induces $i\Delta_s^{in}$ pairing. In the bottom panel, a current term $iJf_i c_j^\dagger$ following SOC $i\lambda c_j \sigma_z f_i^\dagger$ induces spin polarized $M^{in} \sigma_z$. **d**, The Josephson currents $I(\phi)$ in unit of $\frac{2e}{h}$ for the $\Delta_d + i\Delta_s$ JD. **e**, Band structures for Nb_3Br_8 TB with wavefunction projections onto each layer. From wavefunction projection, layer 1 and layer 2 strongly couple with each other and form an insulator with band gap. Layer 3 is metallic with bandwidth 0.1eV. The other parameters are set as $\Delta_{s0} = 0.05$, $\Delta_d = 0.03$, $t_R = t_L = 1.0$, $\Delta_R = \Delta_L = 0.2$, $t_{RB} = 0.8$, $t_{LB} = 0.4$, $\mu = -3.0$. In the calculation, we set the thickness of SC on both sides to be 20.

are discussed in the supplemental materials [17].

Following the above procedure, the proximity process for TB with a $d_{x^2-y^2} + is$ wave pairing ($i\Delta_s \sum_i f_{i\uparrow} f_{i\downarrow} + \Delta_d \sum_{<i,j>} (-1)^{i_y-j_y} c_i c_j + h.c.$) and Δ_R under current flow $iJ \sum_{<i,j>} c_i^\dagger f_j + h.c.$ is calculated. Importantly, the current J term can induce a $i\Delta_s^{in}$ component towards the TB layer through the proximity process as well. This effect can be understood from a perturbation approach, as illustrated in the up panel of Fig.4c. $iJf_{i\sigma} < c_{j\sigma}^\dagger c_{j\sigma}^\dagger > t_{RB}f_{i\sigma}$ perturbation process induces an effective $i\Delta_s$ pairing proportional to $t_{RB}\Delta_R$ since $< c_{j\sigma}^\dagger c_{j\sigma}^\dagger > \propto \Delta_R$. Fig.4b plots the effective spin singlet pairing amplitudes along FS in Fig.4a for $J > 0$ and $J < 0$, which clearly shows the competition between $i\Delta_s$ and the induced $i\Delta_s^{in}$. Therefore, the current flow could tune the proximity region as above. Additionally, the Josephson currents are calculated by Eq.(6) in Fig.4d, which shows a non-reciprocal critical current of the Josephson junction. Hence, a current-controlled JD can be achieved. This nonreciprocal response can also be used to test whether an SC breaks \mathcal{T} symmetry. Furthermore, the current flow may also be used to tune the magnetic order, which is widely used in spintronics [20, 34, 35]. This idea can also be applied to \mathcal{T} breaking JD. For example, the combination of current $iJf_i c_j^\dagger$ and a Kane-Mele type SOC term $i\lambda c_j \sigma_z f_i^\dagger$ [36] can induce an effective spin order term $-J\lambda f_i < c_{j\sigma}^\dagger c_j > \sigma_z f_i^\dagger$, as illustrated in the perturbation approach of Fig.4c.

We can apply our general theory to the JD effect found in the NSB heterostructure. Since NbSe_2 is a conventional s-wave SC [37, 38], the unique feature of NSB JD relies on the Nb_3Br_8 TB. In each conventional cell of bulk Nb_3Br_8 crystal, there are six sub-layers while the NSB only contains three sub-layers to break the \mathcal{I} [16, 39, 40]. Using density functional calculations, we find that the physics of Nb_3Br_8 is dominated by the Nb $d_{z^2-r^2}$ orbital, where two layers are strongly coupled to form a small gap insulator. Therefore, for Nb_3Br_8 TB shown in Fig.4e, layer 1 and layer 2 are insulating with

a metallic layer 3 floating on top of them, which agrees with the geometric setup in Fig.1. More than that, the bandwidth of layer 3 is quite flat with 100meV, which may enlarge the non-reciprocal effect. For the NSB heterostructure, there are two non-reciprocal phenomena related to the finite critical current difference ΔI_c and the finite returning current difference ΔI_r [16]. Hence, we can conclude that the \mathcal{T} breaking must take place due to the nonvanishing ΔI_c . The origin of the \mathcal{T} breaking is likely from its nearly flatband of the metallic layer, which can host a magnetic ground state due to the correlation and the interface competition [17, 41]. The more detailed feature of Nb_3Br_8 calls for further theoretical and experimental investigations. For the ΔI_r , owing to the charge accumulation of the device capacitance, the voltage potential at the interface can change the proximity region to give rise to ΔI_r [16, 28].

In general, the Josephson junction can be understood from the Ginzburg-Landau (G-L) theory [2, 3, 42]. Phenomenologically, the Josephson junction SNS is described by the macroscopic pairing potential ψ_R and ψ_L [42]. The G-L boundary condition at the interface can be written as

$$\frac{\partial \psi_R}{\partial z} = \frac{\psi_L}{b} \quad (7)$$

$$\frac{\partial \psi_L}{\partial z} = -\frac{\psi_R}{b} \quad (8)$$

where the length b is a phenomenological length describing the tunneling barrier. Then the Josephson current is

$$j_s = \frac{2e\hbar}{mb} |\psi_L| |\psi_R| \sin(\phi_L - \phi_R) \quad (9)$$

where the $\phi_{L/R}$ are the corresponding phases for $\psi_{L/R}$ respectively. Therefore, the critical current depends on b and $|\psi_{L/R}|$. If parameter b can be tuned by the external fields, a JD is formed. Although we take an extreme limit with an insulator and metal TB in the above examples, general JDs only rely on symmetry breaking. And tuning b is equivalent to adjusting the proximity region, which can be applied to general designs.

For the JD effects using the magnetochiral anisotropy and the asymmetric edge states, both of them are \mathcal{T} breaking JD [9, 10, 14, 15]. Taking the Rashba system as an example, the magnetic field B_y along the y direction will induce a finite momentum shift q_x along the x direction because of the Rashba SOC ($k_x\sigma_y - k_y\sigma_x$). Owing to this finite momentum, the current flow along the x direction behaves differently in the positive and negative directions, which also shows different proximity processes as above.

In summary, we study the general theory for Josephson diodes. Based on symmetry analysis, there are two types of JDs, \mathcal{I} breaking JD and \mathcal{T} breaking JD. For \mathcal{I} breaking JD, the voltage can be used to control the internal potential dependent quantity, like the Rashba SOC, which leads to $I_c(V) \neq I_c(-V)$. For \mathcal{T} breaking JD, the magnetic field or the current could serve as the controlling parameter, which leads to $I_c(B) \neq I_c(-B)$ or $I_{c+} \neq I_{c-}$. In this case, the tunneling barrier needs to break \mathcal{T} in addition to \mathcal{I} breaking, like the internal magnetism or time-reversal breaking pairing. All these results provide a comprehensive understanding of JD physics and lead to general principles of JD designs. We hope our findings could further stimulate the investigation of Josephson diode effects both theoretically and experimentally.

Note that, when finalizing this work, another zero-field superconducting diode effect has been experimentally observed and theoretically studied in a twisted trilayer graphene and WSe₂ heterostructure [43, 44]. Although the setup is slightly different from that discussed in our work, the underlying physics is the same, where an internal time-reversal symmetry breaking and the interface proximity contribute the nonreciprocal transport [43]. And the flat band of the twisted trilayer graphene may enhance the nonreciprocal effect as in the NSB case.

This work is supported by the Ministry of Science and Technology (Grant No. 2017YFA0303100), National Science Foundation of China (Grant No. NSFC-11888101, No. NSFC-12174428), and the Strategic Priority Research Program of Chinese Academy of Sciences (Grant No. XDB28000000). Y.Z. is supported in part by NSF China Grant No. 12004383 and No. 12074276 and the Fundamental Research Funds for the Central Universities.

* jphu@iphy.ac.cn
 † jiangkun@iphy.ac.cn

[1] J.R. Schrieffer, *Theory of Superconductivity* (Addison-Wesley, Reading, MA, 1964).
 [2] M. Tinkham, *Introduction to Superconductivity* (McGraw-Hill, New York, 1975).
 [3] P. G. de Gennes, *Superconductivity of Metals and Alloys* (Benjamin, New York, 1966).
 [4] P. W. Anderson and J. M. Rowell, “Probable observation of the josephson superconducting tunneling effect,” *Phys. Rev. Lett.* **10**, 230–232 (1963).
 [5] B.D. Josephson, “Possible new effects in superconductive tunnelling,” *Physics Letters* **1**, 251–253 (1962).
 [6] S. M. Sze, *Physics of Semiconductor Devices* (Wiley, New York, 1981).
 [7] Jiangping Hu, Congjun Wu, and Xi Dai, “Proposed design of a josephson diode,” *Phys. Rev. Lett.* **99**, 067004 (2007).
 [8] Kou Misaki and Naoto Nagaosa, “Theory of the nonreciprocal josephson effect,” *Phys. Rev. B* **103**, 245302 (2021).
 [9] Fuyuki Ando, Yuta Miyasaka, Tian Li, Jun Ishizuka, Tomonori Arakawa, Yoichi Shiota, Takahiro Moriyama, Youichi Yanase, and Teruo Ono, “Observation of superconducting diode effect,” *Nature* **584**, 373–376 (2020).
 [10] James Jun He, Yukio Tanaka, and Naoto Nagaosa, “A phenomenological theory of superconductor diodes,” arXiv e-prints, arXiv:2106.03575 (2021), [arXiv:2106.03575 \[cond-mat.supr-con\]](https://arxiv.org/abs/2106.03575).
 [11] Ryohei Wakatsuki, Yu Saito, Shintaro Hoshino, Yuki M. Itahashi, Toshiya Ideue, Motohiko Ezawa, Yoshihiro Iwasa, and Naoto Nagaosa, “Nonreciprocal charge transport in noncentrosymmetric superconductors,” *Science Advances* **3**, e1602390 (2017).
 [12] Yoshinori Tokura and Naoto Nagaosa, “Nonreciprocal responses from non-centrosymmetric quantum materials,” *Nature Communications* **9**, 3740 (2018).
 [13] Akito Daido, Yuhei Ikeda, and Youichi Yanase, “Intrinsic Superconducting Diode Effect,” arXiv e-prints, arXiv:2106.03326 (2021), [arXiv:2106.03326 \[cond-mat.supr-con\]](https://arxiv.org/abs/2106.03326).
 [14] Noah F. Q. Yuan and Liang Fu, “Supercurrent diode effect and finite momentum superconductivity,” arXiv e-prints, arXiv:2106.01909 (2021), [arXiv:2106.01909 \[cond-mat.supr-con\]](https://arxiv.org/abs/2106.01909).
 [15] Chui-Zhen Chen, James Jun He, Mazhar N. Ali, Gil-Ho Lee, Kin Chung Fong, and K. T. Law, “Asymmetric josephson effect in inversion symmetry breaking topological materials,” *Phys. Rev. B* **98**, 075430 (2018).
 [16] Heng Wu, Yaojia Wang, Pranava K. Sivakumar, Chris Pasco, Stuart S. P. Parkin, Yu-Jia Zeng, Tyrel McQueen, and Mazhar N. Ali, “Realization of the field-free Josephson diode,” arXiv e-prints, arXiv:2103.15809 (2021), [arXiv:2103.15809 \[cond-mat.supr-con\]](https://arxiv.org/abs/2103.15809).
 [17] See Supplemental Material for more detailed discussions.
 [18] E.I. Rashba, “Symmetry of bands in wurzite-type crystals. 1. symmetry of bands disregarding spin-orbit interaction,” *Sov. Phys. Solid. State* **1**, 368 (1959).
 [19] Y. A. Bychkov and E.I. Rashba, “Properties of a 2d electron gas with lifted spectral degeneracy,” *JETP Lett.* **39**, 78 (1984).
 [20] A. Manchon, H. C. Koo, J. Nitta, S. M. Frolov, and R. A. Duine, “New perspectives for rashba spin-orbit coupling,” *Nature Materials* **14**, 871–882 (2015).
 [21] F.T. Vasko, “Spin splitting in the spectrum of two-dimensional electrons due to the surface potential,” *JETP Lett.* **30**, 541 (1979).
 [22] Junsaku Nitta, Tatsushi Akazaki, Hideaki Takayanagi, and Takatomo Enoki, “Gate control of spin-orbit interaction in an inverted $in_{0.53}ga_{0.47}as/in_{0.52}al_{0.48}as$ heterostructure,” *Phys. Rev. Lett.* **78**, 1335–1338 (1997).
 [23] M. Ben Shalom, M. Sachs, D. Rakhmievitch, A. Palevski, and Y. Dagan, “Tuning spin-orbit coupling and superconductivity at the $srto_3/laalo_3$ interface: A magnetotransport study,” *Phys. Rev. Lett.* **104**, 126802 (2010).
 [24] A. F. Andreev, “The thermal conductivity of the intermediate state in superconductors,” *Sov. Phys. JETP* **19**, 1228 (1964).
 [25] B. Pannetier and H. Courtois, “Andreev reflection and proximity effect,” *Journal of Low Temperature Physics* **118**, 599–615 (2000).
 [26] C. W. J. Beenakker and H. van Houten, “Josephson current

through a superconducting quantum point contact shorter than the coherence length,” *Phys. Rev. Lett.* **66**, 3056–3059 (1991).

[27] P. W. Anderson and H. Hasegawa, “Considerations on double exchange,” *Phys. Rev.* **100**, 675–681 (1955).

[28] Kenya Ohgushi, Shuichi Murakami, and Naoto Nagaosa, “Spin anisotropy and quantum hall effect in the kagomé lattice: Chiral spin state based on a ferromagnet,” *Phys. Rev. B* **62**, R6065–R6068 (2000).

[29] Rahul Nandkishore, L. S. Levitov, and A. V. Chubukov, “Chiral superconductivity from repulsive interactions in doped graphene,” *Nature Physics* **8**, 158–163 (2012).

[30] Wan-Sheng Wang, Yuan-Yuan Xiang, Qiang-Hua Wang, Fa Wang, Fan Yang, and Dung-Hai Lee, “Functional renormalization group and variational monte carlo studies of the electronic instabilities in graphene near $\frac{1}{4}$ doping,” *Phys. Rev. B* **85**, 035414 (2012).

[31] Yong Ren, Ji-Hai Xu, and C. S. Ting, “Ginzburg-landau equations for mixed s+d symmetry superconductors,” *Phys. Rev. B* **53**, 2249–2252 (1996).

[32] Masashige Matsumoto and Hiroyuki Shiba, “Co-existence of different symmetry order parameters near a surface in d-wave superconductors iii,” *Journal of the Physical Society of Japan* **65**, 2194–2203 (1996).

[33] Q. P. Li, B. E. C. Koltenbah, and Robert Joynt, “Mixed s-wave and d-wave superconductivity in high- t_c systems,” *Phys. Rev. B* **48**, 437–455 (1993).

[34] Igor Žutić, Jaroslav Fabian, and S. Das Sarma, “Spintronics: Fundamentals and applications,” *Rev. Mod. Phys.* **76**, 323–410 (2004).

[35] Atsufumi Hirohata, Keisuke Yamada, Yoshinobu Nakatani, Ioan-Lucian Prejbeanu, Bernard Diény, Philipp Pirro, and Burkard Hillebrands, “Review on spintronics: Principles and device applications,” *Journal of Magnetism and Magnetic Materials* **509**, 166711 (2020).

[36] C. L. Kane and E. J. Mele, “ Z_2 topological order and the quantum spin hall effect,” *Phys. Rev. Lett.* **95**, 146802 (2005).

[37] E. Revolinsky, G.A. Spiering, and D.J. Beerntsen, “Superconductivity in the niobium-selenium system,” *Journal of Physics and Chemistry of Solids* **26**, 1029–1034 (1965).

[38] H.F. Hess, R.B. Robinson, and J.V. Wasczak, “Stm spectroscopy of vortex cores and the flux lattice,” *Physica B: Condensed Matter* **169**, 422–431 (1991).

[39] Christopher M. Pasco, Ismail El Baggari, Elisabeth Bianco, Lena F. Kourkoutis, and Tyrel M. McQueen, “Tunable magnetic transition to a singlet ground state in a 2d van der waals layered trimerized kagomé magnet,” *ACS Nano* **13**, 9457–9463 (2019).

[40] Yuanfeng Xu, Luis Elcoro, Guowei Li, Zhi-Da Song, Nicolas Regnault, Qun Yang, Yan Sun, Stuart Parkin, Claudia Felser, and B. Andrei Bernevig, “Three-Dimensional Real Space Invariants, Obstructed Atomic Insulators and A New Principle for Active Catalytic Sites,” arXiv e-prints , arXiv:2111.02433 (2021), [arXiv:2111.02433 \[cond-mat.mtrl-sci\]](https://arxiv.org/abs/2111.02433).

[41] Junke Jiang, Qiuhua Liang, Ruishen Meng, Qun Yang, Chun-jian Tan, Xiang Sun, and Xianping Chen, “Exploration of new ferromagnetic, semiconducting and biocompatible nb₃x₈ (x = cl, br or i) monolayers with considerable visible and infrared light absorption,” *Nanoscale* **9**, 2992–3001 (2017).

[42] S. N. Song, *Superconductivity* (Cambridge University Press, Cambridge, 1999).

[43] Jiang-Xiazi Lin, Phum Siriviboon, Harley D. Scammell, Song Liu, Daniel Rhodes, K. Watanabe, T. Taniguchi, James Hone, Mathias S. Scheurer, and J. I. A. Li, “Zero-field superconducting diode effect in twisted tri-layer graphene,” arXiv e-prints , arXiv:2112.07841 (2021), [arXiv:2112.07841 \[cond-mat.mes-hall\]](https://arxiv.org/abs/2112.07841).

[44] Harley D. Scammell, J. I. A. Li, and Mathias S. Scheurer, “Theory of zero-field diode effect in twisted tri-layer graphene,” arXiv e-prints , arXiv:2112.09115 (2021), [arXiv:2112.09115 \[cond-mat.mes-hall\]](https://arxiv.org/abs/2112.09115).

Supplemental Material for General theory of Josephson Diodes

CRYSTAL STRUCTURES AND ELECTRONIC STRUCTURES OF Nb_3Br_8

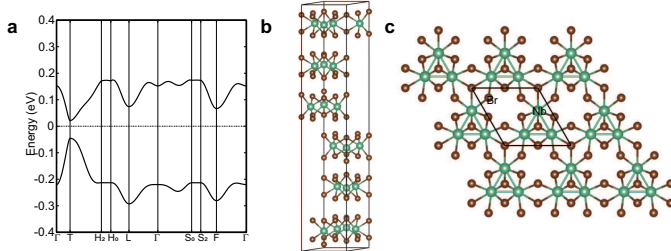


FIG. S1. (color online) **a**, The DFT-calculated band structure of Nb_3Br_8 . **b**, The crystal structure of Nb_3Br_8 from side view. **c**, The structure of one layer in Nb_3Br_8 .

The crystal structure of Nb_3Br_8 is shown in Fig. S1b: six Nb_3Br_8 layers stack along [001] direction, forming its conventional cell. In Nb_3Br_8 , Nb is coordinated with 6 Br atoms and NbBr_6 octahedral complexes connects each other by sharing edges. Thus, the Nb_3Br_8 monolayer can be viewed as a distorted version of CdI_2 -type layer with $\frac{1}{4}$ vacancies. Moreover, Nb atoms in Nb_3Br_8 will trimerize, as shown in Fig. S1c, leading that half of Nb-Nb bonds shorten (2.87 Å) while the other half of bonds elongate (4.23 Å). As a result, Nb atoms form a distorted kagome lattice in Nb_3Br_8 monolayer. Although there are six layers in Nb_3Br_8 conventional cell, there are only two inequivalent layers in its primitive cell because of its 12R stacking structure[S1]. This is consistent the result of the band calculation: there are two bands around the Fermi level, attributed to two distinctive Wannier functions (WFs) centered in Nb_3 triangles in two layers. These two bands are relatively flat, owing to the relatively long Nb-Nb bonds between triangles (4.23 Å).

We build a trilayer Nb_3Br_8 model with 40 Å thick vacuum layer, which has been realized experimentally[S2]. The scenario changes here. The WF in layer-1 and the WF in layer-2 are centered in the same site, as shown in Fig. S2c,d. These two WFs strongly coupled, forming the highest and lowest band in Fig. S2a. The rest layer is metallic, forming the half-occupied band in Fig. S2a.

COMPUTATIONAL DETAILS

Our density functional theory (DFT) calculation is performed for the triplelayer Nb_3Br_8 together with built-in 40 Å thick vacuum layer by Vienna ab initio simulation package (VASP) code[S3] with the projector augmented wave (PAW) method[S4]. The Perdew-Burke-Ernzerhof (PBE)[S5] exchange-correlation functional is used in our calculation.

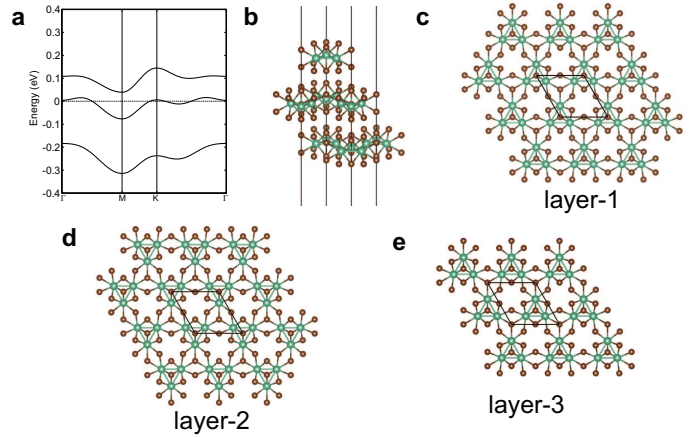


FIG. S2. (color online) **a**, The DFT-calculated band structure of trilayer Nb_3Br_8 . **b**, The crystal structure of trilayer Nb_3Br_8 from side view. **c-e**, The crystal structure of each layer in trilayer Nb_3Br_8 .

The kinetic energy cutoff is set to be 600 eV for the expanding the wave functions into a plane-wave basis. The energy convergence criterion is 10^{-7} eV and the Γ -centered \mathbf{k} -mesh is $12 \times 12 \times 2$. The triplelayer Nb_3Br_8 is fully relaxed while forces are minimized to less than 0.001 eV/Å. The zero-damping DFT-D3 method is used to consider vdW interaction[S6].

Wannier90 code[S7, S8] is employed to calculate maximally localized Wannier functions (MLWFs) centered in Nb_3 triangular clusters.

MORE GENERAL \mathcal{T} BREAKING CASE

In our model calculation, we consider a cubic lattice with Josephson current direction along z axis, so that the system is still translation invariant in the x - y plane. We use a 20×20 \mathbf{k} -mesh in the x - y plane and consider 41 unit cell along z direction which consists of right and left superconducting region with thickness of 20 and one single layer representing the tunneling barrier (TB). We have performed the calculation with denser \mathbf{k} -mesh and larger thickness along the z direction and the results do not change qualitatively.

Pure is wave pairing case

In the main text, we show the Josephson diode effect of TB with a $d_{x^2-y^2} + is$ wave pairing. Here we show in Fig. S3 that similar effect can also be achieved in the case of TB with pure is wave pairing, since the key physics is the competition between the induced $i\Delta_s^{in}$ and $i\Delta_s$ in the TB. In this calculation, the parameters used are the same as those used in Fig. 4 of the main text except that the d-wave pairing strength Δ_d is set to 0 to realize a pure is wave pairing in TB.

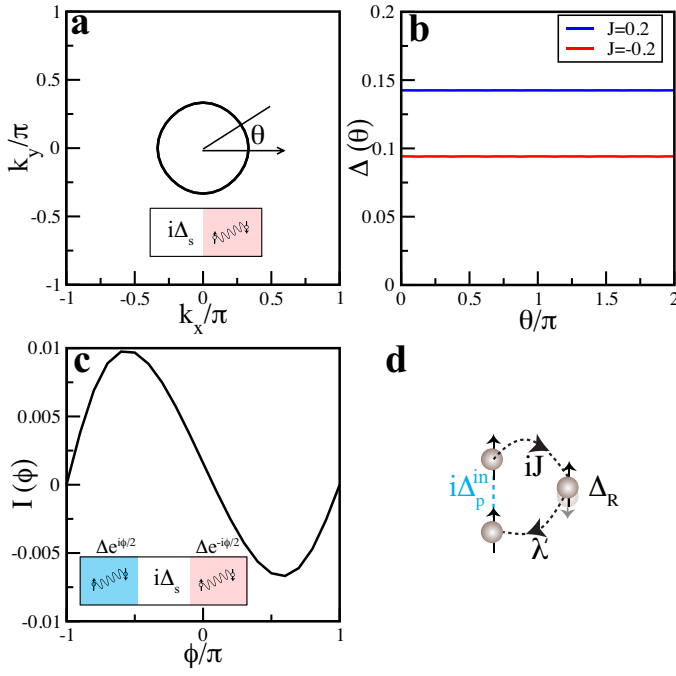


FIG. S3. (color online) **a**, Fermi surface for TB with $i\Delta_s$ pairing. The inset illustrates the proximity process leading to the pairing amplitude in **b**. **b**, Spin singlet pairing strengths along each FS for $J = \pm 0.2$. θ is the angle along each FS as defined in **a**. **c**, The Josephson currents $I(\phi)$ in unit of $\frac{2e}{h}$ for the $i\Delta_s$ JD. **d**, Perturbation process for $i\Delta_p$ pairing. A current term $iJ f_{i\sigma} c_{i'\bar{\sigma}}^\dagger$, a pairing term $c_{i'\sigma}^\dagger c_{i'\bar{\sigma}}^\dagger$, followed by $\lambda' c_{i'\bar{\sigma}}^\dagger f_{j\bar{\sigma}}$ SOC induces $i\Delta_p^{in}$ pairing.

s+ ip wave pairing case

If the TB has $s + ip$ wave pairing, the system can also have diode effect through the p wave pairing induced by the current. The mechanism of the induced p wave pairing

can be understood from the following perturbation process: $iJ f_{i\sigma} < c_{i'\sigma}^\dagger c_{i'\bar{\sigma}}^\dagger > \lambda' f_{j\sigma}$ where we have introduced a nearest neighbour spin-orbit coupling λ' between the fermion $f_{j\sigma}$ in the TB and the fermion $c_{i'\bar{\sigma}}^\dagger$ in the bulk superconductor. This induced p wave pairing amplitude Δ_p^{in} is proportional to $iJ\lambda'\Delta_R$ since $< c_{j\sigma}^\dagger c_{j\bar{\sigma}}^\dagger > \propto \Delta_R$, which can compete with the $s+ip$ wave pairing in the TB depending on the sign of the current. This process is illustrated schematically in Fig. S3a.

Another contribution of the effective p wave pairing comes from the even higher order perturbation process that involves the Rashba coupling inside the TB, which comes from the term $iJ f_{i\sigma} c_{i'\sigma}^\dagger t c_{i'\bar{\sigma}}^\dagger f_{i\bar{\sigma}} (-ia f_{i\bar{\sigma}}^\dagger (\boldsymbol{\sigma} \times \mathbf{d}_{ij})_z^{\bar{\sigma}\sigma} f_{j\sigma}) \propto Jt\alpha\Delta_R < f_{i\bar{\sigma}} f_{i\bar{\sigma}}^\dagger > (\boldsymbol{\sigma} \times \mathbf{d}_{ij})_z^{\bar{\sigma}\sigma} f_{i\bar{\sigma}} f_{j\sigma}$, so that the effective p wave pairing amplitude is proportional to $Jt\alpha\Delta_R$ and has the $p_x + ip_y$ like phase structure.

* jphu@iphy.ac.cn

† jiangkun@iphy.ac.cn

- [S1] K. Habermehl and G. Meyer, Zeitschrift für Naturforschung B **65**, 770 (2010).
- [S2] H. Wu, Y. Wang, P. K. Sivakumar, C. Pasco, S. S. Parkin, Y.-J. Zeng, T. McQueen, and M. N. Ali, arXiv preprint arXiv:2103.15809 (2021).
- [S3] G. Kresse and J. Furthmüller, Comput. Mater. Sci. **6**, 15 (1996).
- [S4] G. Kresse and D. Joubert, Phys. Rev. B **59**, 1758 (1999).
- [S5] J. P. Perdew, K. Burke, and M. Ernzerhof, Phys. Rev. Lett. **77**, 3865 (1996).
- [S6] S. Grimme, J. Antony, S. Ehrlich, and H. Krieg, The Journal of chemical physics **132**, 154104 (2010).
- [S7] A. A. Mostofi, J. R. Yates, Y.-S. Lee, I. Souza, D. Vanderbilt, and N. Marzari, Comput. Phys. Commun. **178**, 685 (2008).
- [S8] N. Marzari, A. A. Mostofi, J. R. Yates, I. Souza, and D. Vanderbilt, Reviews of Modern Physics **84**, 1419 (2012).